The Journal of Chemical Physics

Intrinsic water layering next to soft, solid, hydrophobic, and hydrophilic substrates

Cite as: J. Chem. Phys. **153**, 224702 (2020); https://doi.org/10.1063/5.0030021
Submitted: 18 September 2020 • Accepted: 18 November 2020 • Published Online: 09 December 2020

Meng Chen, Lin Li, Runliang Zhu, et al.

The Journal of Chemical Physics ARTICLE scitation.org/journal/jcp

Intrinsic water layering next to soft, solid, hydrophobic, and hydrophilic substrates

Cite as: J. Chem. Phys. 153, 224702 (2020); doi: 10.1063/5.0030021
Submitted: 18 September 2020 • Accepted: 18 November 2020 •
Published Online: 9 December 2020

Meng Chen,[1,a)] Lin Li,[1,2] Runliang Zhu,[1,2] Jianxi Zhu,[1,2] and Hongping He[1,2]

AFFILIATIONS

[1]CAS Key Laboratory of Mineralogy and Metallogeny/Guangdong Provincial Key Laboratory of Mineral Physics and Materials, Guangzhou Institute of Geochemistry, Institutions of Earth Science, Chinese Academy of Sciences (CAS), Guangzhou 510640, China
[2]University of Chinese Academy of Sciences, Beijing 100049, China

[a)]**Author to whom correspondence should be addressed:** chenmeng@gig.ac.cn

ABSTRACT

How a substrate modulates properties of water upon it and how far the perturbation is present remain to be fundamental questions in surface science. To answer these questions, we develop a layer-by-layer exfoliation method to identify physically meaningful water layers upon a substrate through molecular dynamics simulations under ambient conditions. The results show a qualitatively consistent long-ranged layer-by-layer propagation of the atomic structure, irrespective of whether the substrate is soft, solid, hydrophobic, or hydrophilic. The capillary-wave fluctuation of a water layer upon air or oil diverges with long wavelength but is truncated upon solid substrates by an effective field, which exhibits a long-ranged decay but its strength is almost irrelevant with substrate chemistry. The distinction in the water structure and atomic dynamics due to substrate specificity is mostly limited to the outmost layer. We conclude a long-ranged layering organization and a short-ranged substrate-dependent specificity for interfacial water.

I. INTRODUCTION

Aqueous interfaces are ubiquitous in nature and technology, and are of great interest in electrochemistry, geochemistry, environmental science, and atmospheric science.[1,2] The structure of water next to a surface is distinct from that of bulk water, thus leading to the specificity in water dynamics,[3–5] charge transfer,[6–8] dielectric response,[9–11] and heterogeneous ice nucleation mechanism.[12–15] Unambiguously characterizing the topology of water molecules and collective dynamics next to a surface and disclosing how far the surface perturbation extends into buried water[1] are the fundamentals of understanding surface specificity.

A hydrophobic solid substrate and a hydrophilic one, which are classified by the contact angle of a water droplet on it,[16] exert distinct influences on water structure and especially the orientation of molecules.[17] Beyond hydrophilicity, the chemical heterogeneity of a substrate modulates water dynamics.[18,19] Besides, if the substrate is a soft matter, e.g., hydrophobic oil,[5,20] it allows a long-ranged fluctuation of surface water. Surface rigidity, hydrophilicity, and chemistry are variables that could alter the water–substrate interactions. On the other hand, the water–water interaction, which includes hydrogen-bond (HB) and van der Waals interactions,[21] competes with the water–substrate interaction and probably minimizes the specificity. To what extent does the surface specificity modulate the structure and dynamics? At what distance are structure and dynamics commensurate with those of bulk water? Is there a universality in structure and dynamics of interfacial water?

Surface-sensitive vibrational spectroscopy, e.g., vibrational sum frequency generation (SFG), combined with molecular dynamics (MD) simulations, has been utilized to study the air/water and buried solid/aqueous interface.[22–29] SFG, which depends on the second-order susceptibility, is forbidden in media with inversion symmetry (bulk liquid) but allowed at interfaces. The spectrum has contributions from both the so-called binding interfacial layer (BIL) and diffuse layer (DL); the former is in direct contact with the surface boundary, while the latter is close to bulk water but modulated by the interfacial field.[30–33] It provides information such as dipole orientation,[25,28,34] hydrogen-bond structure,[26,35]

hydrogen-bond relaxation,[24,36] and the order of water next to a surface.[27] Layering of water on a substrate derived by the density profile in the laboratory frame through the combined X-ray reflectivity (XRR) and MD/MC (Monte Carlo) simulation approach seems to reflect the depth of interfacial water, which is more or less 1.0 nm.[37–40] However, this density oscillation in the laboratory frame might not reflect the intrinsic water layering, because the spatial and temporal fluctuations of a water layer might blur the intrinsic structure.

In order to show the specificity of water next to a substrate, the intrinsic surface of water should be characterized first. Water layering can be recognized by the density profile on the basis of the intrinsic surface, named an intrinsic density profile.[20] Willard and Chandler defined the instantaneous surface through a set of points on the coarse-grained density field whose value is equal to half of the bulk density.[41,42] On the basis of the instantaneous surface, they showed a long-ranged distinction in intrinsic density profiles between water next to a hydrophilic substrate and a hydrophobic one.[42] The Willard and Chandler definition on the instantaneous surface has been relied on explaining the structure and charge transfer of water next to different substrates.[6,23,43] Through analyzing the structure of water based on the instantaneous surface by *ab initio* MD simulations, Pezzotti *et al.* divided BIL, DL, and bulk water, and showed that the combination of BIL and DL, which is within a few Å from the interfacial boundary, is responsible for the SFG signal.[31,32] Since the SFG technique is just sensitive to media whose inversion symmetry is broken in the laboratory frame, is it possible that there is water beyond the DL still interfered by the interface but presenting an inversion symmetry in the laboratory frame? Or is it possible that the DL is much deeper than previously thought but the broken symmetry of the deeper part is so faint to be recognized? Most importantly, whether the Willard and Chandler method is accurate enough in defining the intrinsic surface, which could alter the derivation based on it?

Tarazona and Chacón had showed that, if an intrinsic surface is based on the local Gibbs dividing surface, the intrinsic density profile becomes unphysical because the bulk interference blurs the surface fluctuation.[44] The local Gibbs dividing surface is derived with local density profiles. The Willard and Chandler method makes use of a coarse-grained density field, i.e., a field of local density.[41] As both methods are based on local density, it casts doubt on the accuracy of the Willard and Chandler method. Alternatively, the intrinsic sampling method (ISM) by Tarazona and Chacón to define the intrinsic surface is through molecular recognition. The intrinsic surface disclosed by the ISM is in accordance with the description of capillary wave theory (CWT).[45–47] As will be shown in results, the difference between intrinsic density profiles of water next to hydrophilic and hydrophobic substrates with the ISM is not as distinct as that Willard and Chandler showed.[42]

Unlike dividing interfacial water into BIL and DL, we see interfacial water as a propagation of molecular layers, which manifest themselves as peaks in the intrinsic density profile. Besides a reliable definition of the intrinsic surface, whether the intrinsic density profile really decodes the intrinsic layering of interfacial water depends on two assumptions: (1) a strong layer-by-layer coupling such that inner layers can be similarly identified as the outmost one; (2) a nearly homogeneous water distribution among a layer such that the density averaged over a layer is similar to the local one. Because a weak layer-by-layer coupling interferes with decoding structure of inner layers, we develop a layer-by-layer exfoliation method to identify outmost and inner layers at the same time. As well as the intrinsic density profile based on the outmost layer surface, those

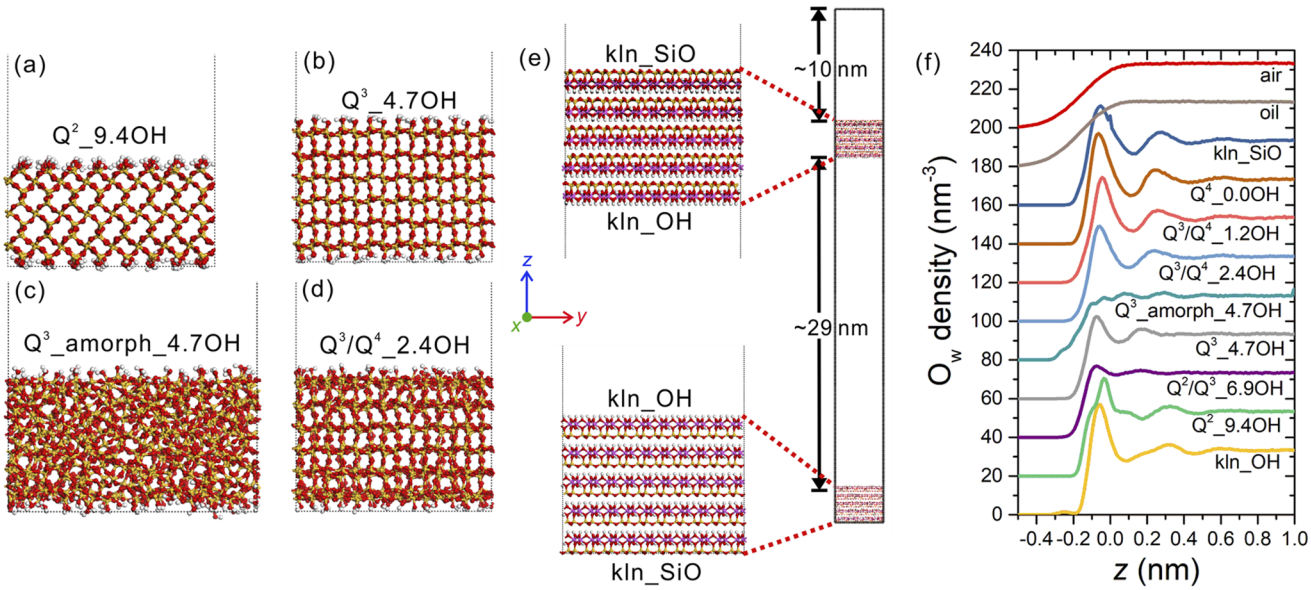

FIG. 1. Selected substrate models [(a)–(e)] and density profiles of water O atoms in the laboratory frame (f). Si, Al, O, and H atoms in the models are in yellow, purple, red, and white, respectively. The profiles have been offset for clarity.

TABLE I. Summary of simulation systems in this study.

System	Size [$L_x \times L_y \times L_z$ (nm)][a]	Water-slab thickness (nm)
Air/water	4.63 × 4.47 × 30.00	~9
Oil/water	4.63 × 4.47 × 26.96	~10
kln_OH and kln_SiO/water	4.63 × 4.47 × 46.36	~29 and ~10
Q^2_9.4OH/water	3.47 × 3.43 × 11.34	~8
Q^2/Q^3_6.9OH/water	3.34 × 3.49 × 12.16	~7
Q^3_4.7OH/water	3.34 × 3.49 × 12.11	~7
Q^3_amorph_4.7OH/water	4.03 × 4.14 × 11.70	~8
Q^3/Q^4_2.4OH/water	3.34 × 3.49 × 12.06	~7
Q^3/Q^4_1.2OH/water	3.34 × 3.49 × 12.00	~7
Q^4_0.0OH/water	3.34 × 3.49 × 12.04	~7

[a]L_x and L_y refer to the dimensions of the original model, and they are not adjusted during simulations. L_z refers to the equilibrium value after the NP_zT run.

based on inner layer surfaces are also derived, which unambiguously discloses the structural propagation through layers. The surface perturbation on water is shown to be well beyond the traditionally thought 1.0 nm.

The influences of surface rigidity, hydrophilicity, and chemistry on the layer-by-layer propagation are systematically investigated here. Water/air, water/oil interfaces, and water next to solid substrates with different hydrophilicities and atomic configurations were studied (Fig. 1 and Table I). The hydrophobic and hydrophilic (001) surfaces of kaolinite[48] and silica surfaces with different hydrophilicities and atomic configurations[49] were used as substrates. The following sections are organized as follows: (1) In the methodology section, we show MD simulation details, the method for a layer-by-layer identification with MD simulation trajectories, and how layer-by-layer dynamic properties are derived. (2) In Sec. III, we first show how the identified layer meets the physically meaningful criteria and disclose the capillary-wave fluctuations of layers. (3) Second, we show the long-ranged layer-by-layer propagation of structural properties including atomic density, hydrogen-bond (HB) structure, molecular order, and dipole orientations. (4) Third, the layer-by-layer dynamic properties are presented. (5) In the discussion section, we discuss the influences with different surface definitions and show the interconversion between local density, intrinsic density, and laboratory density profiles. Through this study, the universality and specificity in the layer-by-layer structural and dynamical evolution of water next to different substrates are disclosed. We conclude a long-ranged layering organization but a short-ranged substrate-dependent specificity for interfacial water. This work may hopefully set the framework for analyzing the interfacial liquid.

II. METHODOLOGY

A. Simulation models

The model of an air/water interface was built through inserting a water slab into a vacuum box which is much thicker than the slab. The oil/water and silica/water interfaces were constructed through stacking a water slab on top of a dodecane slab and a silica substrate, respectively. Thus, due to the periodic boundary condition, it gave rise to two substrate/water interfaces. Charge-free silica substrates were adopted from the surface model database[49] and were named Q^2_9.4OH, Q^2/Q^3_6.9OH, Q^3_4.7OH, Q^3_amorph_4.7OH, Q^3/Q^4_2.4OH, Q^3/Q^4_1.2OH, and Q^4_0.0OH, respectively. Q^2, Q^3, and Q^4 refer to different surface environments, which are two silanol groups per superficial Si atom [$=Si(OH)_2$], one silanol group per superficial Si atom [$\equiv Si(OH)$], and no silanol group per superficial Si atom, respectively. Q^2/Q^3 or Q^3/Q^4 implies that a surface is mixed with Q^2 and Q^3 or Q^3 and Q^4 environments. The Q^2_9.4OH surface is derived from the (100) cleavage plane of α-quartz and contains 9.4 silanol groups/nm^2. Q^2/Q^3_6.9OH, Q^3_4.7OH, Q^3/Q^4_2.4OH, Q^3/Q^4_1.2OH, and Q^4_0.0OH surfaces are derived from the $(10\bar{1})$ cleavage plane of α-cristobalite, and they contain 6.9, 4.7, 2.4, 1.2, and 0.0 silanol groups/nm^2, respectively. Q^3_amorph_4.7OH is a substrate of amorphous silica with 4.7 silanol groups/nm^2. This silanol density approximates that of Zhuravlev's model (4.6 or 4.9 silanol groups/nm^2).[50] The (001) surfaces of kaolinite consist of a hydrophobic siloxane surface and a hydrophilic hydroxyl one,[48] which are referred to as kln_SiO and kln_OH, respectively. Two 9 × 5 × 5 supercells of the kaolinite crystal[51] were reversely inserted into a vacuum box [Fig. 1(e)], as done in previous studies.[52,53] Subsequently, two water slabs were inserted into the two vacuum spaces of the box, giving rise to a kln_SiO/water and a kln_OH/water interface. The thickness of the water slab between the two kln_OH surfaces is set to as large as ~29 nm to disclose the long-ranged orientational order of water dipoles. Representative substrate models can be seen in Fig. 1. The system sizes can be seen in Table I.

B. Simulation settings

The SPC/E,[54] TraPPE,[55] INTERFACE,[49] and ClayFF[56] force fields were used to describe water, dodecane, silica, and kaolinite, respectively. The cutoff radius for Lennard-Jones potential was set

to 1.98 nm for the air/water, oil/water, and kaolinite/water systems, while it was set to 1.60 nm for the silica/water systems. The particle–mesh Ewald (PME) method[57,58] was used to describe long-ranged electrostatic interactions. Periodic boundary conditions were applied in all directions. MD simulations were performed with the GROMACS 5.1 package.[59] The air/water system was simulated in a canonical (NVT) ensemble for 20 ns. The other systems were simulated in an NP_zT ensemble (only the z dimension was scaled according to a target pressure) for 10 ns at first and then were subsequently simulated in an NVT ensemble for 10 ns. The time step was 1 fs. Temperature was coupled to 300 K, while pressure in the z dimension was coupled to 1.0 bar. The Nosé–Hoover thermostat[60,61] and Parrinello–Rahman barostat[62,63] were used to couple temperature and pressure, respectively. Data were collected every 1 ps in the last 10 ns simulations for analysis.

C. Identification of intrinsic layers

We anticipate a layer-by-layer stacking of water molecules next to a substrate. A layer is constructed by the collection of water molecules at an instance. An intrinsic surface is an instantaneous description of a layer, as described in the laboratory frame by the equation: $z = \xi(\boldsymbol{R}, \lambda_c)$, where $\boldsymbol{R} = (x, y)$. $\xi(\boldsymbol{R}, \lambda_c)$ can be written as a Fourier expansion form as follows:

$$\xi(\boldsymbol{R}, \lambda_c) = \sum_{|\boldsymbol{q}| \le 2\pi/\lambda_c} \hat{\xi}_q e^{i\boldsymbol{q}\boldsymbol{R}}, \tag{1}$$

where $\boldsymbol{q}$ is a wave vector and expressed as $\boldsymbol{q} = 2\pi(\mu/L_x, \nu/L_y)$, in which $\mu, \nu = 0, \pm1, \pm2, \ldots$.[45] L_x and L_y are lengths of the simulation box in x and y directions, respectively. λ_c is the cutoff wavelength, as set to λ_m, which is 0.317 nm approximating the molecular size of water.[46] Equation (1) can be transformed into cosine/sine functions,

$$\xi(x, y, \lambda_c) = \sum_{\mu,\nu} a_{\mu\nu} f_\mu(x) f_\nu(y), \tag{2}$$

in which $f_0(x) = 1$, $f_\mu(x) = \cos(2\pi\mu x/L_x)$, and $f_{-\mu}(x) = \sin(2\pi\mu x/L_x)$, for $\mu > 0$, and $f_0(y) = 1$, $f_\nu(y) = \cos(2\pi\nu y/L_y)$, and $f_{-\nu}(y) = \sin(2\pi\nu y/L_y)$, for $\nu > 0$. μ and ν fulfill the condition $(\mu/L_x)^2 + (\nu/L_y)^2 \le 1/{\lambda_c}^2$. We denote the number of summation terms as n_a. $a_{\mu\nu}$ are real coefficients remained to be solved. If $a_{\mu\nu}$ are derived, the intrinsic surface can be mathematically reproduced with Eq. (2).

We utilized the ISM[45–47] to construct an intrinsic surface of a water layer. The center of mass of a water molecule is used to represent its position. Based on molecular positions, a list of liquid water molecules was built for each frame of the simulation trajectory. Any molecule with less than three neighbors of water molecules within a distance of $1.5\lambda_m$ was seen as a gas molecule and was not present on the list. Then, the cross section of the box was divided into 5×5 grids. When constructing the outmost water layer, in each grid, the outmost molecule from the liquid list was selected. As a result, $N_l = 25$ primary molecular pivots were determined. These pivots were used to construct a surface described by Eqs. (1) or (2) with $\lambda_c = \lambda_m$. The surface was required to be as close to pivot sites as possible, and the surface area should be minimized at the same time. These two goals were compromised through minimizing the following function:

$$W = \frac{1}{2}\sum_{i=1}^{N_l} (z_i - \xi(\boldsymbol{R}_i, \lambda_m))^2 + \frac{\varepsilon L_x L_y}{2} \sum_{|\boldsymbol{q}| \le 2\pi/\lambda_m} q^2 \left|\hat{\xi}_q\right|^2. \tag{3}$$

The first term in Eq. (3) was for building a surface as close to pivot sites as possible, while the second term was for minimizing the surface area. A marginal deviation of the surface from pivot sites was allowed through setting ε to be a non-zero value. ε was set to 1.0×10^{-8} here, which was consistent with previous studies.[46] Minimizing W introduced n_a linear equations with the same form as

$$\sum_{\mu',\nu'} a_{\mu'\nu'} \sum_{i=1}^{N_l} f_\mu(x_i) f_\nu(y_i) f_{\mu'}(x_i) f_{\nu'}(y_i) + 4\pi^2 \psi(\mu, \nu) \varepsilon a_{\mu\nu} L_x L_y \left[\left(\frac{\mu}{L_x}\right)^2 + \left(\frac{\nu}{L_y}\right)^2\right] = \sum_{i=1}^{N_l} z_i f_\mu(x_i) f_\nu(y_i), \tag{4}$$

in which $\psi(\mu, \nu) = 0.5$ if $\mu = 0$ or $\nu = 0$, $\psi(\mu, \nu) = 1$ if both $\mu = 0$ and $\nu = 0$, otherwise $\psi(\mu, \nu) = 0.25$. Through solving n_a linear equations with the form of Eq. (4), $a_{\mu\nu}$ were derived. Thus, a primary surface $\xi(x, y, \lambda_c)$ [Eq. (2)], which was constructed by $N_l = 25$ pivots, was established. After the construction of the primary surface, a new water molecule from the liquid list locating closest to the surface was added into the pivot list, leading to $N_l = 26$. Then, the surface was reconstructed with 26 pivots through solving n_a linear equations with the form of Eq. (4) again. Finding a new pivot molecule, increasing N_l by one, and reconstructing a surface were repeated. When N_l reached the optimal value N_o, the surface of a physically meaningful outmost layer was established. N_o was set such that pivot molecules composing the layer exhibited collective dynamics, which separate them from thermal motions of other molecules as far as possible. The determination of N_o, the only parameter which matters in the ISM, is important, which would be explained in detail in Sec. III A.

After the outmost layer was constructed, the second layer was built in succession. Water molecules belonging to the outmost layer were excluded from the liquid list. Then, the second layer was established with a similar method through selecting $N_l = 5 \times 5$ pivot molecules at first and adding pivot molecules and reconstructing the surface through solving Eq. (4) until the optimal pivot number N_o was achieved. Similarly, more inner layers were established. In this study, up to ten layers were built for water on each substrate. The work flow of the above procedures for layer-by-layer identification can be seen in Fig. 2.

D. Derivations of layer-by-layer translational and reorientational dynamics

In each system, 1000 snapshots recorded every 10 ps during the 10 ns equilibrium run were selected to begin microcanonical (NVE) simulations. Each NVE simulation lasted for 10 ps. Data were saved every 0.01 ps. Thus, 1000 independent NVE trajectories of the same system were for deriving the average dynamic property. Translational dynamics were quantified by diffusion coefficients perpendicular and parallel to the interface ($D_\perp$ and $D_\parallel$).[64,65] $D_\parallel$ was

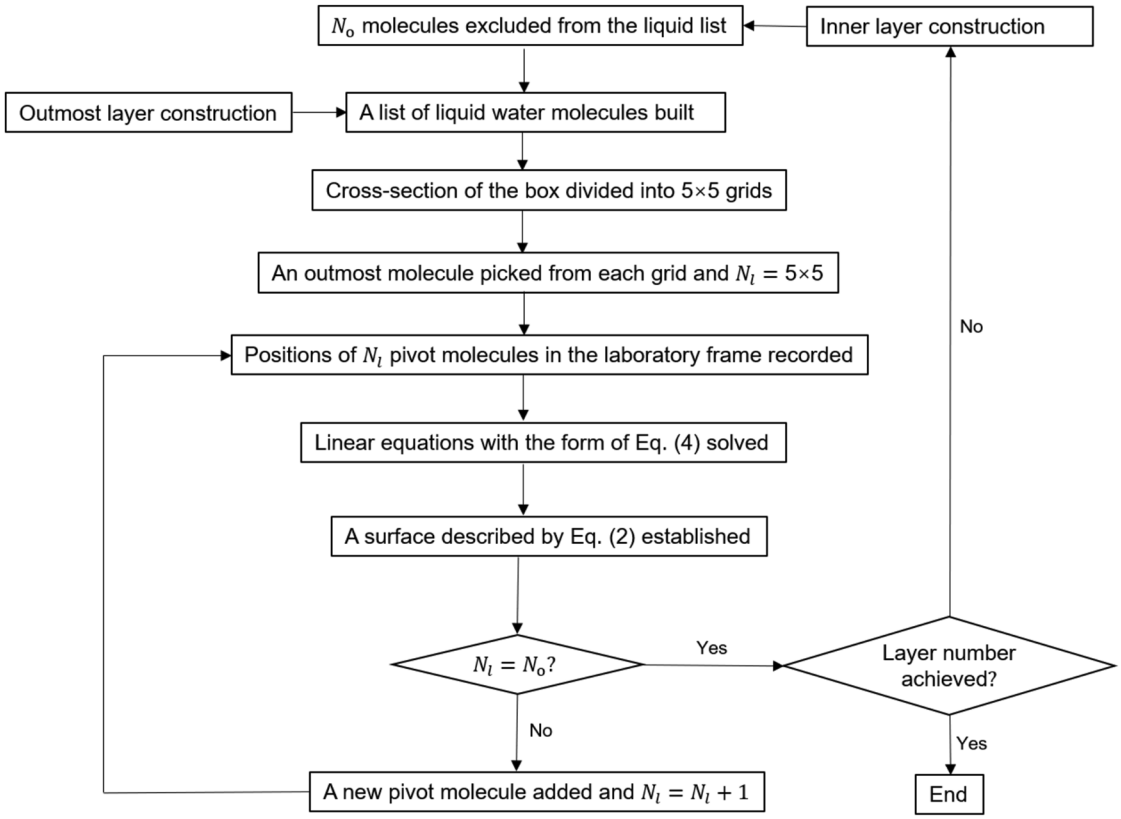

FIG. 2. The work flow of procedures for instantaneous layer-by-layer identification.

calculated with the equation $D_{\parallel} = \lim_{t\to\infty} \frac{\langle \Delta r_{\parallel}^2 \rangle_{\Omega}}{2tP(t)}$, in which $\langle \Delta \boldsymbol{r}_{\parallel}^2 \rangle_{\Omega}$ is the mean square displacement in the plane parallel to the interface averaged over molecules persistently located in layer Ω and $P(t)$ is the survival probability at time t for a molecule in Ω.[65] $P(t)$ was calculated with $P(t) = \langle n(0) \cdot n(t) \rangle_{\Omega}$, in which n can be either 0 or 1, depending on whether or not a molecule leaves layer Ω. In the beginning of an NVE simulation, a molecule was judged to be in a specific layer according to the layer-by-layer identification techniques as explained above. Thence, whether a molecule was still judged to be in the layer at time t was according to the effective position and thickness of the layer in the laboratory frame, avoiding high computational cost for identifying intrinsic layers from massive NVE trajectories. The effective layer position was $\hat{\xi}_0$ in Eq. (1) derived through the equilibrium NVT simulation. The effective layer thickness L was approximated by $2 \times L_{\mathrm{FWHM}}$, in which L_{FWHM} was the full width at half maximum (FWHM) of the positional probability distribution of an intrinsic surface in the z dimension of the laboratory frame (Fig. S7 in the supplementary material). If a molecule was in $\hat{\xi}_0 \pm L/2$ from time 0 to t, $n(t)$ was 1, otherwise it was 0. The short data-collecting interval (0.01 ps) during an NVE simulation ensured the correctness of $P(t)$. $\langle \Delta \boldsymbol{r}_{\parallel}^2 \rangle_{\Omega}/P(t)$, which represents the translational dynamics in the plane parallel to the interface, was averaged over all NVE trajectories for a system. On the other hand, $D_{\perp}$ can be calculated with $D_{\perp} = -\lim_{t\to\infty} \frac{L^2 \ln[P(t)]}{\alpha t}$, in which α is a parameter related to the distribution of water.[65] As intrinsic density profiles were similar in all cases as will be shown below, we did not derive the exact value of α and assumed that it is almost invariant across different cases. We averaged $-L^2 \ln[P(t)]$ over all NVE trajectories for a system to show the possible difference in perpendicular translational dynamics. The NVE trajectories were also for deriving reorientational dynamics of water. The reorientation time correlation function $C_{2,\mathrm{reor}}$ is expressed as $C_{2,\mathrm{reor}} = \langle P_2[\boldsymbol{u}(0) \cdot \boldsymbol{u}(t)] \rangle$, in which P_2 is the second-order Legendre polynomial and $\boldsymbol{u}$ is the orientation of a water OH bond. According to the extended jump model, the reorientation of a water OH bond is separated into a frame reorientation and a jump reorientation due to a HB exchange.[66] The frame-reorientation time correlation function $C_{2,\mathrm{frame}}$ is defined as $C_{2,\mathrm{frame}} = \langle P_2[\boldsymbol{u}(0) \cdot \boldsymbol{u}(t)] \rangle_{\text{no exchange}}$, which accounts for the reorientation of an OH bond persistently donating a HB to an acceptor. With $C_{2,\mathrm{reor}}$ and $C_{2,\mathrm{frame}}$ derived for water from different layers, reorientational dynamics with and without HB exchanges were systematically disclosed.

III. RESULTS AND DISCUSSIONS

A. Layer-by-layer identification for interfacial water

According to CWT,[67] the wave vector dependent fluctuation of a layer is expressed as

$$\left\langle \left| \hat{\xi}_q \right|^2 \right\rangle = \frac{k_B T}{[V_0 + \gamma(q) q^2] A_0}, \tag{5}$$

in which A_0 is the cross-sectional area, V_0 is the effective field strength, and $\gamma(q)$ is the wave vector dependent surface tension and expressed as $\gamma(q) = \gamma_0 + \kappa q^2 + \cdots$. γ_0 and κ are the same as the macroscopic surface tension and bending modulus, respectively. If higher-order terms of $\gamma(q)$ can be neglected, Eq. (5) is rewritten as

$$\left\langle \left| \hat{\xi}_q \right|^2 \right\rangle A_0 = \frac{k_B T}{V_0 + \gamma_0 q^2 + \kappa q^4}. \tag{6}$$

For a free layer which is not under the influence of an external field, $V_0 = 0$ and the capillary-wave fluctuation diverges in the $q = 0$ limit. This long-wavelength divergence is eliminated if $V_0 > 0$. $\hat{\xi}_q$ are the same as those in Eq. (1). When the intrinsic surface mathematically described by Eq. (2) is derived, the conversion from Eq. (2) to Eq. (1) discloses $\hat{\xi}_q$. Thus, the relationship between $\left\langle \left| \hat{\xi}_q \right|^2 \right\rangle$ and q can examine if the fluctuation of the constructed surface obeys CWT.

The key to identify an intrinsic layer with the ISM is with an optimal N_o. The best choice of N_o should give rise to a physically meaningful water layer, which meets the following criteria: (1) the collective dynamics of water composing the layer are independent from bulk dynamics as far as possible; (2) the mesoscopic fluctuation of the layer conforms to the CWT description, i.e., Eqs. (5) or (6); (3) the intrinsic density profile based on the intrinsic layer surface is as sharp as possible.[45–47] In the following, we will first show how N_o are determined for intrinsic layers of water next to air.

Criterion (1) is tested through calculating the molecular flux Φ as a function of N_l (Fig. 3). Φ is defined as the number of water molecules that enter or depart a layer per unit time.[46] When constructing the outmost water layer next to air, there is a minimum of Φ [Fig. 3(a)], which corresponds to N_l molecules whose collective dynamics are separated from bulk dynamics to the maximum extent. Thus, we take N_l at the minimum of Φ to be N_o. On the other hand, we also find that Criterion (2) is met as the mesoscopic fluctuation of the layer constructed by N_o pivots conforms to Eq. (6), the CWT description. We use γ_0 derived with macroscopic pressure tensors ($\gamma_0 = L_z[\langle P_{zz}\rangle - (\langle P_{xx}\rangle + \langle P_{yy}\rangle)/2]/2$) and $V_0 = 0$ to fit $\left\langle \left| \hat{\xi}_q \right|^2 \right\rangle (q^2)$ with Eq. (6). It exhibits a good fitting [Fig. 4(a)]. The choice of N_o is not sensitive to the long-wavelength fluctuation, which is controlled by γ_0, but it is sensitive to the short-wavelength fluctuation as controlled by κ (Fig. S1 in the supplementary material). As to Criterion (3), we will show that the intrinsic layer consisting of N_o molecules gives rise to a sharp presentation of an intrinsic density profile in Sec. III B. The determination of N_o for the outmost water layer next to air can also be referred to Tarazona and Chacón's study.[47]

Inner layers have not been identified in previous studies. We find that the molecular flux with N_l does not exhibit a minimum when identifying inner layers [Figs. 3(a) and 3(b)]. Yet, Φ is not linear with N_l, and there is seemingly a plateau in $\Phi(N_l)$. As a linear response of Φ to N_l is anticipated for bulk water, it implies that water molecules comprising an inner layer show collective dynamics. It evidences that an inner layer is physically meaningful. Thus, the inflection point of $\Phi(N_l)$ [Figs. 3(a) and 3(b)] should more or less correspond to N_o. We also test the choice of N_o on the derived capillary-wave spectrum of an inner layer, finding that the long-wavelength fluctuation ($\left\langle \left| \hat{\xi}_q \right|^2 \right\rangle$ of a small q) is not sensitive to N_o (Fig. S1 in the supplementary material), being consistent with that of the outmost layer. However, the short-wavelength fluctuation is sensitive to N_o. We anticipate that either γ_0 or κ is consistent through layers, and thus, the short-wavelength spectrum can be examined if N_o is optimal. The optimal N_o which presents a short-wavelength

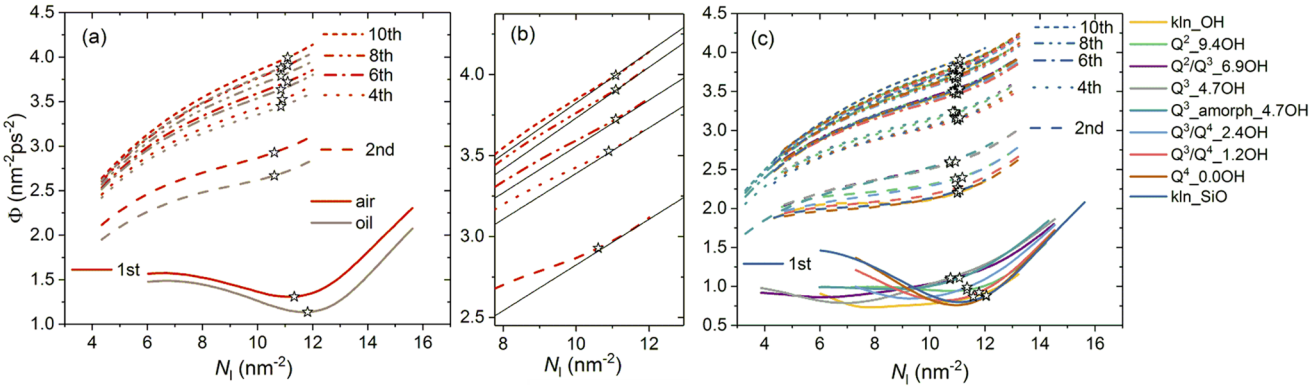

FIG. 3. The fluxes (Φ) of molecules as a function of N_l for water in different layers next to different substrates. The star denotes the optimal N_l value N_o. (a) is for water next to air and oil. (b) shows the enlargement of Φ at high N_l for water next to air. A linear fitting of $\Phi(N_l)$ (solid line) helps identify the inflection point corresponding to N_o. (c) is for water next to solid substrates.

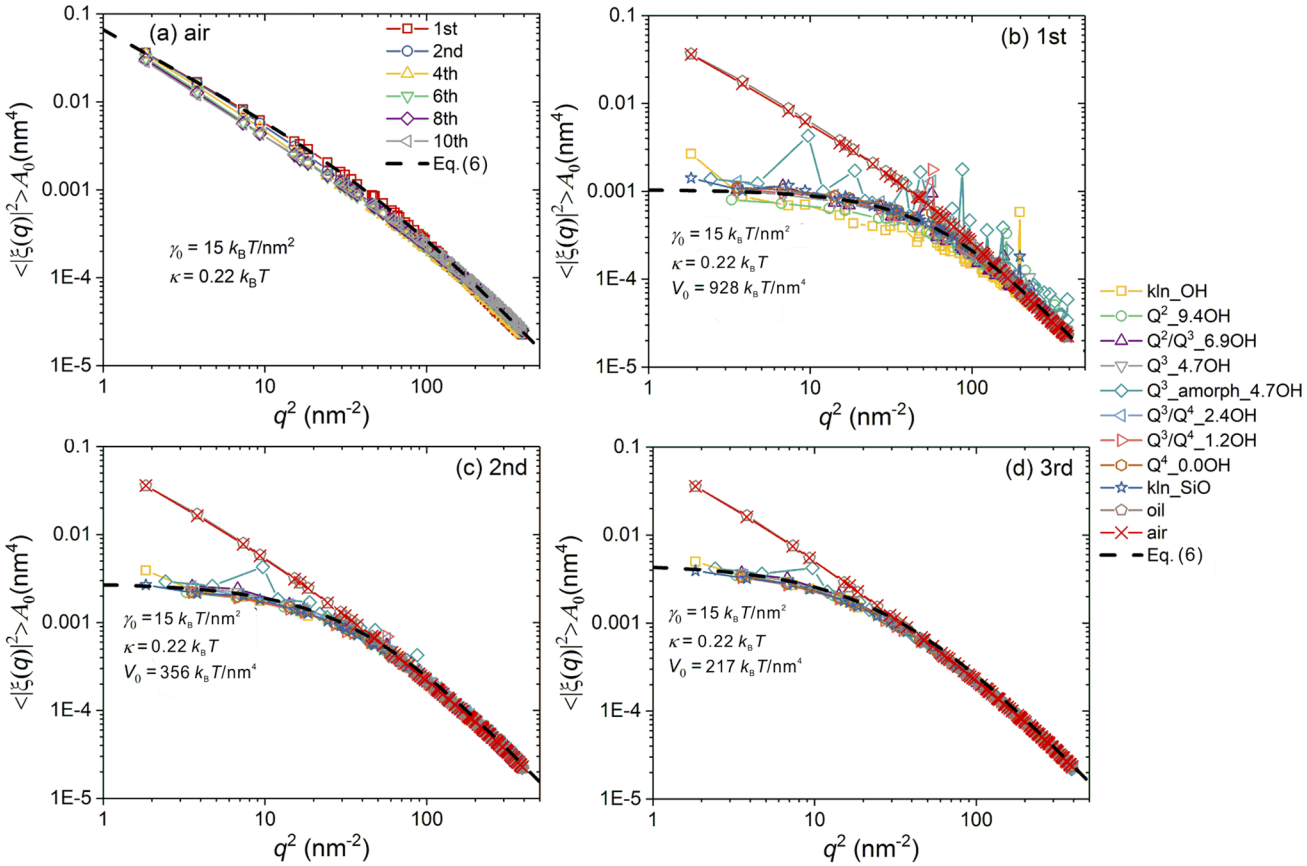

FIG. 4. Mean square amplitude of the Fourier component as a function of q^2 for water layers next to different substrates. (a) is for water layers next to air. (b), (c), and (d) are the cases of the first, second, and third layers of water next to different substrates, respectively.

spectrum for an inner layer [Fig. 4(a)] consistent with that for the outmost one almost coincides with the inflection point of $\Phi(N_1)$ [Figs. 3(a) and 3(b)]. Thus, rigorous determinations of N_o and identifications of water layers next to air are available. In Sec. III B, we will show that such an identification of a layer gives rise to a sharp presentation of an intrinsic density profile based on an inner layer.

Similarly, N_o for water layers next to oil and solid substrates are determined. N_o is not necessary referred to the minimum of $\Phi(N_1)$, but it corresponds to the inflection point in $\Phi(N_1)$ [Figs. 3(a) and 3(c)]. With N_o, the short-wavelength spectrum is qualitatively consistent independent of the substrate chemistry and whether it is for the outmost or an inner layer [Figs. 4(b)–4(d) and Fig. S2 in the supplementary material].

A similar capillary-wave divergence as q decreases is observed for water layers next to air or oil (Fig. 4). However, such a divergence is truncated for water next to any solid substrate [Figs. 4(b)–4(d) and Fig. S2 in the supplementary material]. It implies the influence of an effective field V_0, which retards the long-wavelength fluctuation. The capillary-wave spectrum for a water layer upon a solid substrate can be more or less fitted with Eq. (6) using the same γ_0 and κ as those for water next to air, and thus, a definite V_0 is derived. Despite the local heterogeneity, the spectra for a certain water layer upon different solid substrates largely collapse onto a single function with the same γ_0, κ, and V_0 [Figs. 4(b)–4(d)]. The variation of V_0 with the average depth (d) of a layer shows that V_0 decreases from the outmost layer to inner ones (Fig. 5). Except V_0 for the outmost layer, $V_0(d)$ can be fitted with an exponential function $V_0 = A\exp(-d/d_0) + C$, which is shown in Fig. 5. The term of a constant C unveils a long-ranged non-vanishing V_0. We have calculated capillary-wave spectra for as many as ten water layers. Even the spectrum for the tenth layer upon the solid, which is located at as far as ~3.0 nm from the surface, does not collapse onto that for water next to air [Fig. S2(h) in the supplementary material]. Thus, the addition of an approximately planar solid surface leads to a long-ranged reorganization of water, as unpredicted based on the density profile in the laboratory frame.[37–40] Although the solid substrates cover a range of hydrophilicities as determined by different surface densities of silanol groups,[18,26,49] we show here a consistent long-ranged layering organization of interfacial water.

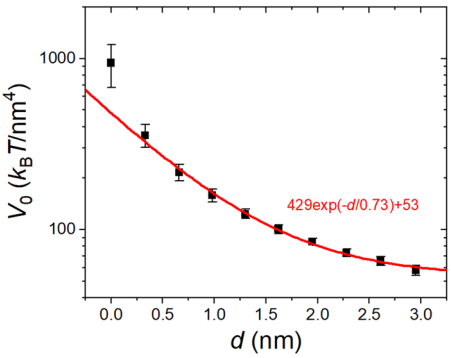

FIG. 5. The effective field strength for water layers as a function of the depth (d) of a layer. d is defined as the position of a specific layer [$\tilde{\xi}_0$ in Eq. (1)] relative to that of the outmost layer. $V_0(d)$ is fitted with a function (red line) explained in this figure.

The local deviation from the single fitting function is most obvious in the capillary-wave spectrum of the outmost layer next to a solid substrate [Fig. 4(b)], while it becomes vanished in those of inner layers [Figs. 4(c) and 4(d) and Fig. S2 in the supplementary material]. A heterogeneity in the spectrum, i.e., a local protrusion at certain q, is present, which corresponds to the chemical heterogeneity of a solid surface. The most heterogeneities appear for the outmost water layer next to the amorphous silica substrate (Q^3_amorph_4.7OH), due to the heterogeneous amorphous surface. The heterogeneity can be visualized by the time-averaged surface of an intrinsic layer (Fig. 6). The surface of the outmost layer next to a crystalline substrate exhibits an ordered undulation, which is apparently shaped by the ordered atomic arrangement of a solid surface. This ordered undulation is largely blurred in the surface of the second layer [Fig. 6(a)]. Thus, the heterogeneity in the capillary-wave spectrum is mostly limited to the outmost water layer. The error bar of V_0 also reflects the discrepancy between spectra of layers upon different solid substrates (Fig. 5), being most obvious for the outmost layer.

B. Structural analyses based on intrinsic layers

An intrinsic atomic density profile based on any surface of a layer is calculated with

$$\tilde{\rho}(z) = \left\langle \sum_{i=1}^{N} \delta[z - z_i + \xi(\boldsymbol{R}_i, \lambda_c)] / A_0 \right\rangle, \quad (7)$$

in which i denotes any atom in the system and $\xi(\boldsymbol{R}_i, \lambda_c)$ as described in Eq. (1) is the reference surface position for atom i. λ_c is set to $1.5\lambda_m$ to allow a presentation of the heterogeneity in density distribution. $\tilde{\rho}(z)$ based on consecutive layer surfaces provide an insight into the structural propagation from the substrate surface to the inner aqueous phase [Figs. 7(a)–7(d) and Figs. S3(a)–S3(d) in the supplementary material]. Either the intrinsic density profile of water O atoms [Figs. 7(a)–7(d)] or H atoms [Figs. S3(a)–S3(d) in the supplementary material] shows a long-ranged structural propagation. It is noted that the intrinsic density profile is sensitive to

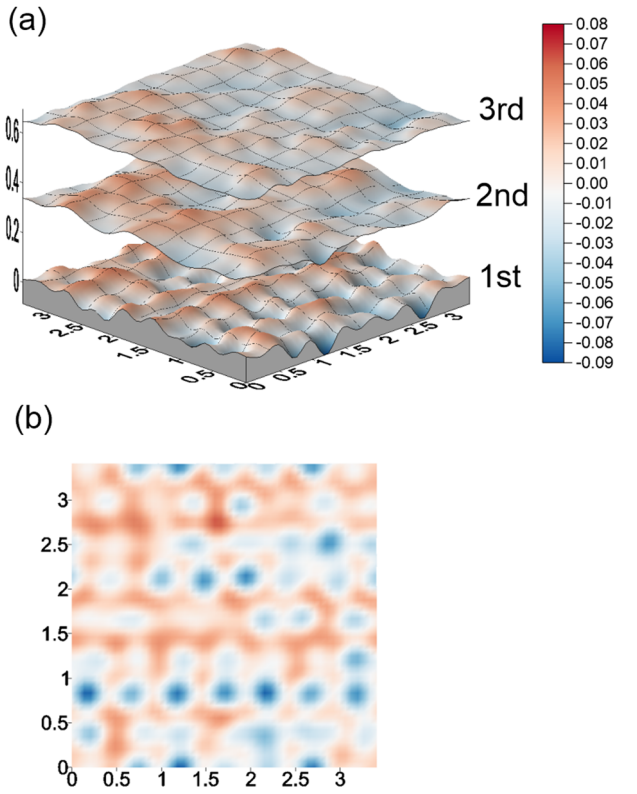

FIG. 6. Intrinsic layer surfaces averaged over a 10 ns simulation for water on the Q^2_9.4OH substrate. The projections of three layer surfaces in the three-dimensional Cartesian space are shown in (a), while the outmost layer surface projected onto the x–y plane is shown in (b). The unit in this figure is nanometer.

the choice of N_o.[46] The underestimation of N_o would lead to a presentation of a left shoulder of the second peak in the profile, while an overestimation leads to the retreating of the second peak (Fig. S4 in the supplementary material). Thus, a sharp presentation of the profile provides another test for the optimal N_o. An optimal intrinsic density profile allows a structural comparison between different water layers upon the same substrate and between layers upon different substrates. Surprisingly, irrespective of the substrate property, the intrinsic density oscillation based on any layer surface exhibits the same frequency [Figs. 7(a)–7(d)]. It is in contrast to the result based on the instantaneous surface with the Willard and Chandler method, which showed a distinct water layering on a hydrophilic substrate.[42] Moreover, except $\tilde{\rho}(z)$ based on the outmost layer exhibiting a substrate-specific heterogeneity, $\tilde{\rho}(z)$ based on any inner layer surface are almost commensurate. Therefore, the surface chemistry just mainly interferes the topology of outmost water molecules. The atomic distribution of water beyond the outmost layer reflects a long-ranged order caused by a surface perturbation, but is less altered by the substrate chemistry.

Other than the atomic density, tetrahedral order (Q), hydrogen-bond (HB) number (N_{HB}), dipole-orientation parameters (p and T) reflect water organizations in different ways (Fig. 7 and Fig. S3 in

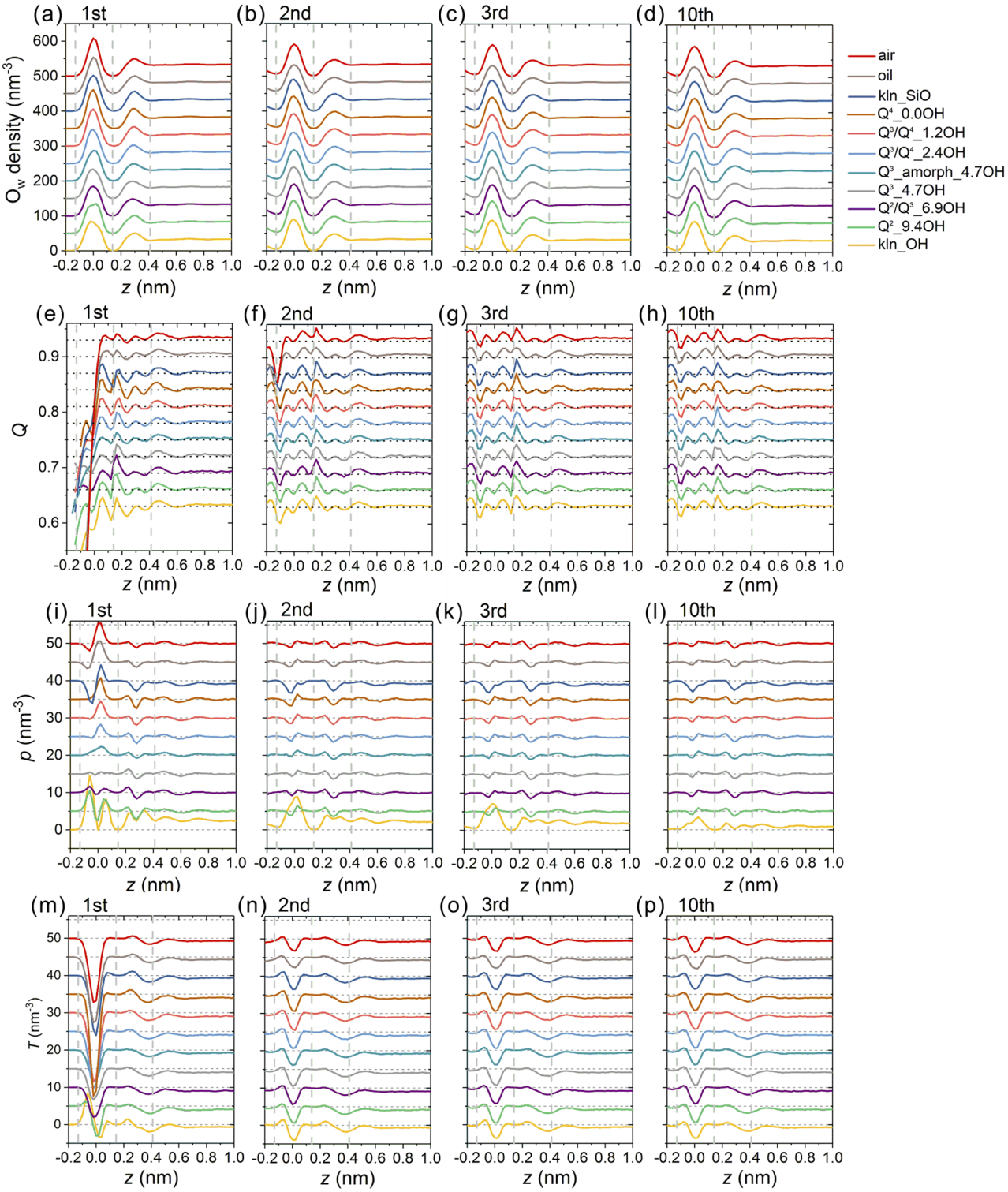

FIG. 7. Intrinsic profiles of density of water O atoms [(a)–(d)], tetrahedral-order parameter (Q) [(e)–(h)], dipole-orientation parameters [p (i)–(l) and T (m)–(p)] based on the surfaces of the first, second, third, and tenth layers. The profiles have been offset for clarity. The dashed vertical lines denote local minima in density profiles of water O atoms.

the supplementary material). Q reflects the ice-like extent and is expressed as $Q = \left\langle 1 - \frac{3}{8}\sum_{j=1}^{3}\sum_{k=j+1}^{4}\left[\cos\left(\psi_{kj}\right) + \frac{1}{3}\right]^2\right\rangle_i$, in which ψ_{kj} is the angle between the vectors connecting the O atom of the water molecule i and the nearest neighbor atoms j and k, which act as HB donors or acceptors.[68] The HB criterion is that the donor–acceptor distance, the hydrogen–acceptor distance, and the hydrogen–donor–acceptor angle are less than 3.5 Å, 2.45 Å, and 30°, respectively.[66] Q as a function of the distance above intrinsic surfaces of outmost and inner layers shows a long-ranged propagation of the tetrahedral order [Figs. 7(e)–7(h)]. Except for $Q(z)$ based on the outmost layer, an almost consistent oscillation of $Q(z)$ based on any layer is observed, irrespective of substrate property. This is also the case for the average number of HBs based on intrinsic surfaces [Figs. S3(e)–S3(h) in the supplementary material]. Different substrates have different HB relationships with outmost water (Fig. S5 in the supplementary material), but HBs between water molecules beyond the outmost layer are less altered by a substrate specificity. p is the projection of the dipole orientation of a water molecule in the z direction,[46] and its sign is related to surface hydrophilicity.[17,26,28] Due to a different substrate hydrophilicity or chemistry, p for the outmost water layer exhibits a substrate-specific distribution [Fig. 7(i)]. However, dipole-orientation oscillations based on inner layer surfaces exhibit similar frequencies and magnitudes [Figs. 7(j)–7(l)], except for water next to a kaolinite surface. Different from other cases, $p(z)$ upon a kaolinite substrate (kln_OH or kln_SiO) bears a significantly higher magnitude and is non-vanishing with z. Because a kaolinite particle bears a net dipole due to its asymmetric structure [Fig. 1(e)], it exerts a long-ranged influence on water orientation, similar to the addition of a static electric field.[69] Even so, the oscillation of $p(z)$ next to a kaolinite surface maintains the same frequency as that next to other substrates. T, which is calculated as $T = (3p^2 - 1)/2$, judges whether the water dipole is perpendicular ($T > 0$) or planar ($T < 0$) to the interface[46] [Figs. 7(m)–7(p)]. It also shows that, except for $T(z)$ based on the first layer, those based on inner water layers upon different substrates are similar. Thus, based on the above analyses, a heterogeneity in the intrinsic structure due to a substrate specificity is just mainly present in outmost water. A long-ranged structural propagation is unaltered by a different substrate, except for the specific long-ranged water-orientation favor next to a substrate with a net dipole.

The combined SFG and MD simulation studies have disclosed structural information of outmost water, e.g., free OH bonds pointing toward the air phase, water accepting HBs from substrate hydrophilic groups, water donating HBs to substrate hydrophobic groups, the HB network between outmost water molecules, and so on.[28,29,32,34,70] Consistent structural information can be observed from the structural analysis based on the outmost intrinsic layer shown here (Fig. 7 and Fig. S5 in the supplementary material). The BIL and DL division has been used to decode SFG signatures.[30–33] The BIL should correspond to the outmost water layer here. The DL by definition corresponds to a region with favorable water orientations but the water structure is almost commensurate with that of bulk water.[31,32] Apparently, the DL would be large for water upon kaolinite surfaces because of a long-ranged non-vanishing dipole favor of water. A previous study has shown a long-ranged contribution to the SFG spectrum for water next to charged graphene,[69] which can also be anticipated for water next to kaolinite. The total width of the BIL and DL was deduced to be just a few Å for water next to silica.[31,32] However, this study shows a long-ranged dipole-orientation propagation through intrinsic layers. This dipole-orientation propagation is probably blurred in the laboratory frame and, thus, hardly detected by the SFG spectrum. Thus, with the layer-by-layer identification method here, the hidden long-ranged structural propagation probably inaccessible by the SFG technique is disclosed.

C. Dynamical analyses based on intrinsic layers

Whether the presence of or the nature of an interface has the largest effect on the dynamics of water molecules has long been asked.[71] The collective dynamics referred to the capillary-wave spectrum are mainly controlled by the presence of a solid substrate, rather than the substrate chemistry, as shown by that even the spectra for the outmost water layers largely collapse onto a master equation [Fig. 4(b)]. However, the local atomic motion is different from the collective dynamics[72] and could be more affected by the substrate specificity, as shown in a study that the coverage and patterning of hydroxyl groups on a silica surface modify molecular diffusion of water.[19] Previous investigations on water dynamics in an inhomogeneous medium were through dividing water molecules based on positions in the laboratory frame.[73,74] Now, we sort water through the layer-by-layer identification. Translational and reorientational dynamics of water are separately investigated. The molecular diffusion in a plane parallel to an interface is quantified by $\langle \Delta \mathbf{r}_{\parallel}^2 \rangle_{\Omega}/P(t)$, which is the mean square displacement in the plane divided by the molecular survival probability in a layer.[65] The diffusion perpendicular to the interface is quantified by $-L^2 \ln[P(t)]$, as accounting for the ability of water molecules leaving a layer with an effective thickness L. Details in deriving the translational dynamics have been shown in Sec. II D. The translational dynamics of water from the outmost layer are obviously impacted by a substrate specificity, as shown by a large divergence across systems with different substrates [Figs. 8(a) and 8(e)]. However, this divergence largely collapses for water in the second layer [Figs. 8(b) and 8(f)]. For water in the third layer and layers beyond it [Figs. 7(c), 7(d), 7(g), and 7(h)], a convergence in translational diffusion can be more or less identified. Reorientational dynamics, as quantified by $C_{2,\mathrm{reor}}$ and $C_{2,\mathrm{frame}}$, which account for the total reorientation of a water OH bond and the reorientation without a HB exchange, also deliver the same picture (Fig. S6 in the supplementary material). A substrate specificity is coupled to atomic dynamics of outmost water due to the HB forming ability and steric effect, which has been deeply investigated before[5,75] and would not be discussed here. The fast convergence of water dynamics from the outmost layer to inner ones is in support of the two-state or core–shell model that describes water dynamics in confinement.[4,76] The outmost intrinsic layer next to a substrate is the shell region, which is mainly responsible for the dynamic heterogeneity.

D. Discussions

With the ISM to perform a layer-by-layer identification for water next to a substrate, we disclose the structural propagation from the outmost to the inner water and the variation of collective

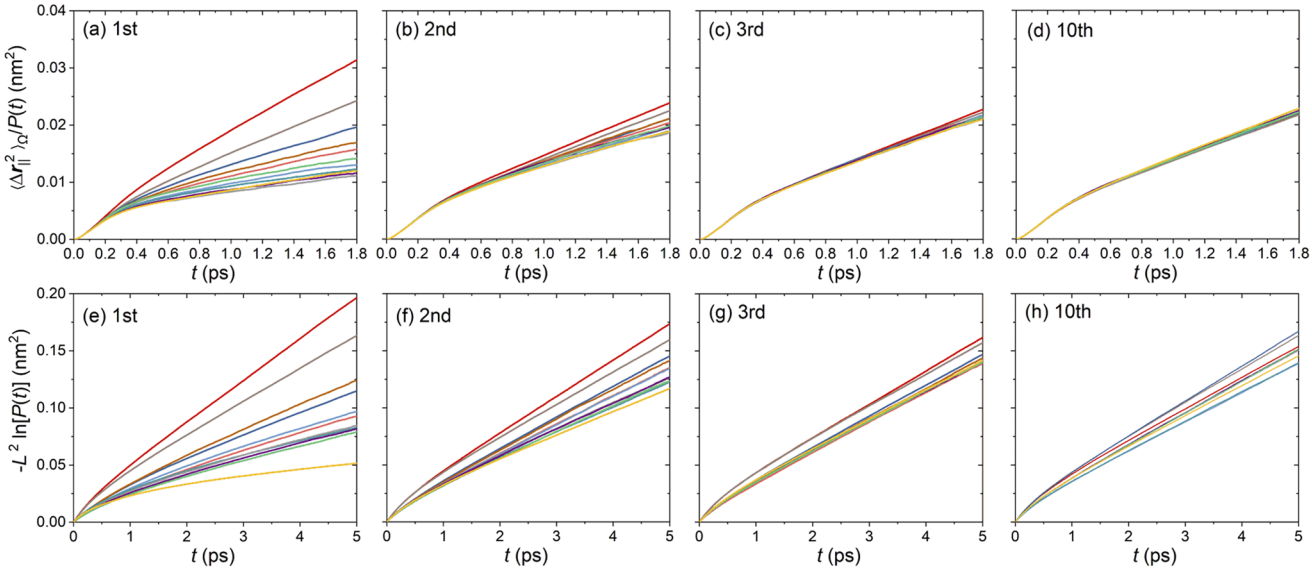

FIG. 8. $\left\langle \Delta r_{\parallel}^2 \right\rangle_\Omega / P(t)$ [(a)–(d)] and $-L^2 \ln[P(t)]$ [(e)–(h)] as functions of time t, which quantify translational water dynamics parallel and perpendicular to the interface, respectively. The line colors denote systems with different substrates as those in Fig. 7.

and atomic dynamics. The ISM just depends on the choice of N_o, which has been shown above to be collectively determined by the inflection point of $\Phi(N_1)$, a consistent short-wavelength capillary-wave fluctuation, and a sharp intrinsic density profile. Thus, it makes the ISM a robust method. We also note the surface reconstruction method (SRM) by Longford *et al.*[77] to amend the intrinsic surface. We compare results with the ISM and SRM in Sec. S1 in the supplementary material. The long-wavelength capillary-wave fluctuation does not vary with different surface construction methods, but the short-wavelength fluctuation with the SRM does not conform to the CWT description (Fig. S8 in the supplementary material). The SRM does not improve the overall sharpness of the intrinsic density profile (Fig. S9 in the supplementary material). Thus, we think it is not necessary to use the SRM other than the ISM.

The variance of the density profile in the laboratory frame [$\rho(z)$] with different substrates [Fig. 1(f)] has long been used to show the specificity in water–substrate interactions.[78] How is it coupled to the intrinsic structure? If the water distribution among a layer is homogeneous, a Gaussian convolution of $\tilde{\rho}(z)$ can reproduce $\rho(z)$,[45,46] which is not the case here (Fig. S10 in the supplementary material). Thus, a heterogeneous water distribution is anticipated. We express a local density as $\rho'(h,z)$, in which h denotes the local position of a surface and z is the distance to the local surface. The local positions of a surface are coarse-grained into h_0, $h_0 + \Delta h$, $h_0 + 2\Delta h \cdots$, in which $\Delta h = 0.05$ nm. Figure 9 shows the decompositions of $\tilde{\rho}(z)$ and $\rho(z)$ into local densities, which clearly explain the difference between hydrophobic kln_SiO and hydrophilic kln_OH substrates. The water distribution is heterogeneous in the outmost layer next to either substrate, as shown by that the centers of local density peaks do not coincide with each other in the intrinsic coordinates. Local density distributions are more irregular for water next to the kln_OH substrate, which make up the density profile in the laboratory frame as a whole being less sharp than that next to the kln_SiO substrate. The sharpness is in terms of the overall profile, as mainly manifested by the first two peaks. The two density peaks in the laboratory frame are distinctly distinguished in the case with the kln_SiO substrate [Fig. 9(b)]. Density decompositions for water next to other substrates can be seen in Fig. S11 and explained in Sec. S2 in the supplementary material. The less sharp profile is a characteristic of a superhydrophilic substrate surface. Although the second peak of $\rho(z)$ is substrate-specific, it is found that this specificity is mainly attributed to the local difference in the outmost intrinsic water layer. Thus, the specificity in $\rho(z)$ is actually caused by the short-ranged difference. $\rho(z)$, as easily determined from molecular simulations and experiments, can be used to determine whether a substrate is superhydrophilic according to its overall sharpness.

Previous studies showed that water in contact with a hydrophobic substrate is characterized by an enhanced compressibility and density fluctuation.[79] The enhanced compressibility corresponds to the regular packing of local density $\rho'(h,z)$ for water next to the hydrophobic substrate disclosed here (Fig. 9 and Fig. S11 in the supplementary material). Irregular packing of local density $\rho'(h,z)$ next to a hydrophilic substrate due to the special HB structure reduces the compressibility. The enhanced density fluctuation can be evidenced by the generally fast translational dynamics of water next to the hydrophobic substrate [Figs. 8(a) and 8(e)]. These phenomena account for local dynamics of water, which are largely modulated by the substrate–water interaction. However, the collective dynamics of outmost water, or the mesoscopic capillary-wave fluctuations, are less altered by the chemistry of a substrate, which reflects an inherent strong water–water interaction. This water–water interaction should be a combination of HB and van der Waals interactions.[21] The

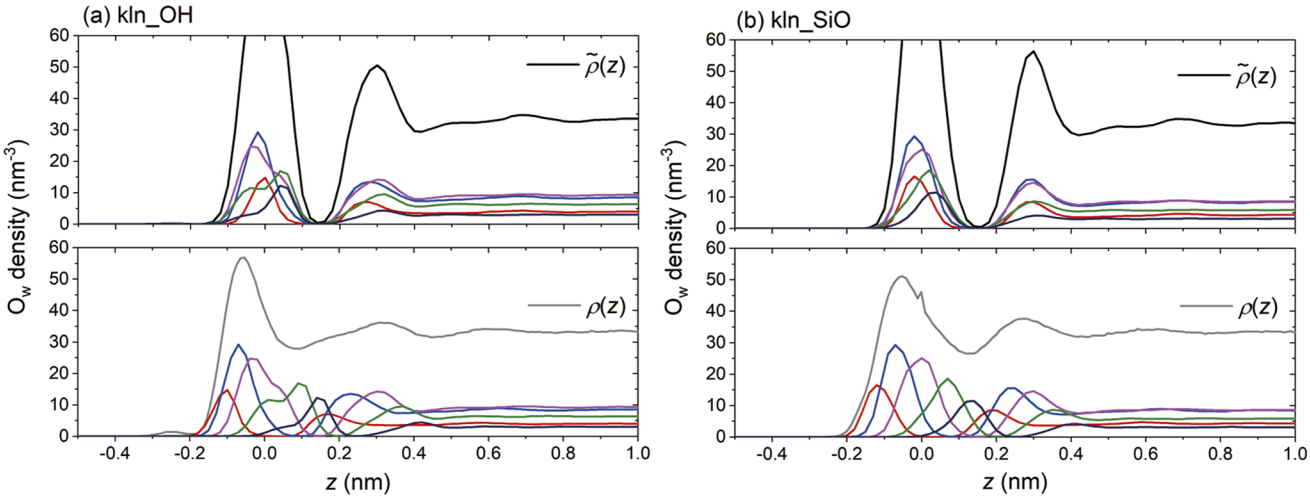

FIG. 9. Decompositions of $\tilde{\rho}(z)$ (black lines) and $\rho(z)$ (gray lines) into local density profiles $\rho'(h,z)$ (colored lines).

consistent structural propagation (water density, tetrahedral order, HB structure, and dipole orientation) (Fig. 7) upon different substrates shown here reflects such a strong water–water interaction. The apparent long-ranged distinction in $\rho(z)$ shown here is mainly due to a short-ranged difference in $\rho'(h,z)$ (Fig. 9 and Fig. S11 in the supplementary material). Similarly, if the intrinsic surface is ill-defined, the superposition of $\rho'(h,z)$ could lead to misleading intrinsic density, $\tilde{\rho}(z)$. The long-ranged distinction between $\tilde{\rho}(z)$ based on instantaneous surfaces upon different substrates with the Willard and Chandler method[31,32,42] might be artificially caused by improper superposition of local density. As centers of local density peaks do not coincide in the intrinsic coordinates as we disclose (Fig. 9 and Fig. S11 in the supplementary material), using points in the laboratory frame with the same coarse-grained local densities to construct an instantaneous surface is less accurate. Analysis based on the Willard and Chandler method has been relied on to decode the SFG spectrum.[23,31,32] Revisiting the layer-by-layer contributions to the SFG spectrum with the method used in this study could hopefully present novel understandings of interfacial water in the future, e.g., a redivision between the BIL and the DL.

Interfacial water is impacted by a substrate property, which is characterized by the surface hydrophilicity, chemistry, and whether the substrate is solid or soft. Moreover, if a substrate bears a net dipole, such as the case of kaolinite, it may exert an external influence as the existence of a static electric field.[69] In this study, the above factors have been investigated. The chemical specificity of a solid substrate surface mainly leads to the distinction in structure and atomic dynamics of the outmost water layer. This distinction rapidly collapses with the depth of an inner water layer. From this point of view, the substrate-specific influence is short-ranged. On the other hand, a long-ranged layer-by-layer propagation of atomic structure and order is identified for water next to either a soft or a solid substrate. Irrespective of a specific solid substrate, the long-wavelength capillary-wave divergence for a certain layer is truncated by a similar effective field, which decays with layer depth but is long-ranged and non-vanishing. It reflects a long-ranged effect, which is only relevant with the substrate geometry but not the substrate chemistry. Upon the substrate with a net dipole, an additional long-ranged non-vanishing favor of water–dipole orientations is observed, as also disclosed in the combined MD and SFG studies of water next to a charged substrate.[69]

IV. CONCLUSIONS

We conclude our main findings for water next to different substrates in the following words: a long-ranged layering organization but a short-ranged substrate-dependent specificity. This study provides a theoretical framework to identify interfacial layering water and shows the structural and dynamical propagations through layers. It could be the foundation for distinguishing short- and long-ranged effects on charge transfer,[6–8,80] dielectric response,[9–11] energy dissipation,[24,81] and ice nucleation[12–15] in interfacial water. Other than water next to solid substrates, water next to soft substrates such as membrane[82] or surfactant monolayer[83] can be investigated in the future. It is also interesting to see how ions solvated in water alter the layer-by-layer structural propagation.

SUPPLEMENTARY MATERIAL

See the supplementary material for the comparison between results with different surface construction methods, the conversion between the intrinsic density profile and the density profile in the laboratory frame, and additional figures in support of the discussion in the main text.

ACKNOWLEDGMENTS

This is contribution No. IS-2946 from GIGCAS. This work was financially supported by the National Natural Science Foundation of China (Grant Nos. 41602034 and 41825003), the Youth Innovation

Promotion Association CAS (Grant No. 2019345), and Science and Technology Planning of Guangdong Province, China (Grant No. 2020B1212060055). We are grateful to the National Supercomputer Center in Guangzhou for the use of high-performance computing facility.

DATA AVAILABILITY

The data that support the findings of this study are available from the corresponding author upon reasonable request.

REFERENCES

[1]O. Björneholm, M. H. Hansen, A. Hodgson, L.-M. Liu, D. T. Limmer, A. Michaelides, P. Pedevilla, J. Rossmeisl, H. Shen, G. Tocci, E. Tyrode, M.-M. Walz, J. Werner, and H. Bluhm, "Water at interfaces," Chem. Rev. **116**, 7698 (2016).
[2]A. Verdaguer, G. M. Sacha, H. Bluhm, and M. Salmeron, "Molecular structure of water at interfaces: Wetting at the nanometer scale," Chem. Rev. **106**, 1478 (2006).
[3]S. Xiao, F. Figge, G. Stirnemann, D. Laage, and J. A. McGuire, "Orientational dynamics of water at an extended hydrophobic interface," J. Am. Chem. Soc. **138**, 5551 (2016).
[4]E. Chiavazzo, M. Fasano, P. Asinari, and P. Decuzzi, "Scaling behaviour for the water transport in nanoconfined geometries," Nat. Commun. **5**, 3565 (2014).
[5]M. Chen, X. Lu, X. Liu, Q. Hou, Y. Zhu, and H. Zhou, "Retardation of water reorientation at the oil/water interface," J. Phys. Chem. C **119**, 16639 (2015).
[6]E. Poli, K. H. Jong, and A. Hassanali, "Charge transfer as a ubiquitous mechanism in determining the negative charge at hydrophobic interfaces," Nat. Commun. **11**, 901 (2020).
[7]J. Lan, V. V. Rybkin, and M. Iannuzzi, "Ionization of water as an effect of quantum delocalization at aqueous electrode interfaces," J. Phys. Chem. Lett. **11**, 3724 (2020).
[8]V. G. Artemov, E. Uykur, P. O. Kapralov, A. Kiselev, K. Stevenson, H. Ouerdane, and M. Dressel, "Anomalously high proton conduction of interfacial water," J. Phys. Chem. Lett. **11**, 3623 (2020).
[9]D. J. Bonthuis, S. Gekle, and R. R. Netz, "Dielectric profile of interfacial water and its effect on double-layer capacitance," Phys. Rev. Lett. **107**, 166102 (2011).
[10]T. Sato, T. Sasaki, J. Ohnuki, K. Umezawa, and M. Takano, "Hydrophobic surface enhances electrostatic interaction in water," Phys. Rev. Lett. **121**, 206002 (2018).
[11]L. Fumagalli, A. Esfandiar, R. Fabregas, S. Hu, P. Ares, A. Janardanan, Q. Yang, B. Radha, T. Taniguchi, K. Watanabe, G. Gomila, K. S. Novoselov, and A. K. Geim, "Anomalously low dielectric constant of confined water," Science **360**, 1339 (2018).
[12]M. Fitzner, G. C. Sosso, S. J. Cox, and A. Michaelides, "The many faces of heterogeneous ice nucleation: Interplay between surface morphology and hydrophobicity," J. Am. Chem. Soc. **137**, 13658 (2015).
[13]A. Haji-Akbari and P. G. Debenedetti, "Perspective: Surface freezing in water: A nexus of experiments and simulations," J. Chem. Phys. **147**, 060901 (2017).
[14]J. Liu, C. Zhu, K. Liu, Y. Jiang, Y. Song, J. S. Francisco, X. C. Zeng, and J. Wang, "Distinct ice patterns on solid surfaces with various wettabilities," Proc. Natl. Acad. Sci. U. S. A. **114**, 11285 (2017).
[15]L. Lupi, A. Hudait, and V. Molinero, "Heterogeneous nucleation of ice on carbon surfaces," J. Am. Chem. Soc. **136**, 3156 (2014).
[16]C. Zhu, H. Li, Y. Huang, X. C. Zeng, and S. Meng, "Microscopic insight into surface wetting: Relations between interfacial water structure and the underlying lattice constant," Phys. Rev. Lett. **110**, 126101 (2013).
[17]S. Shin and A. P. Willard, "Water's interfacial hydrogen bonding structure reveals the effective strength of surface–water interactions," J. Phys. Chem. B **122**, 6781 (2018).
[18]A. M. Schrader, J. I. Monroe, R. Sheil, H. A. Dobbs, T. J. Keller, Y. Li, S. Jain, M. S. Shell, J. N. Israelachvili, and S. Han, "Surface chemical heterogeneity modulates silica surface hydration," Proc. Natl. Acad. Sci. U. S. A. **115**, 2890 (2018).
[19]J. I. Monroe and M. S. Shell, "Computational discovery of chemically patterned surfaces that effect unique hydration water dynamics," Proc. Natl. Acad. Sci. U. S. A. **115**, 8093 (2018).
[20]F. Bresme, E. Chacón, P. Tarazona, and K. Tay, "Intrinsic structure of hydrophobic surfaces: The oil-water interface," Phys. Rev. Lett. **101**, 056102 (2008).
[21]E. Brini, C. J. Fennell, M. Fernandez-Serra, B. Hribar-Lee, M. Lukšič, and K. A. Dill, "How water's properties are encoded in its molecular structure and energies," Chem. Rev. **117**, 12385 (2017).
[22]T. Ishiyama, T. Imamura, and A. Morita, "Theoretical studies of structures and vibrational sum frequency generation spectra at aqueous interfaces," Chem. Rev. **114**, 8447 (2014).
[23]S. Pezzotti, D. R. Galimberti, and M.-P. Gaigeot, "2D H-bond network as the topmost skin to the air–water interface," J. Phys. Chem. Lett. **8**, 3133 (2017).
[24]S. T. van der Post, C.-S. Hsieh, M. Okuno, Y. Nagata, H. J. Bakker, M. Bonn, and J. Hunger, "Strong frequency dependence of vibrational relaxation in bulk and surface water reveals sub-picosecond structural heterogeneity," Nat. Commun. **6**, 8384 (2015).
[25]Y. Tong, F. Lapointe, M. Thämer, M. Wolf, and R. K. Campen, "Hydrophobic water probed experimentally at the gold electrode/aqueous interface," Angew. Chem., Int. Ed. **56**, 4211 (2017).
[26]J. D. Cyran, M. A. Donovan, D. Vollmer, F. Siro Brigiano, S. Pezzotti, D. R. Galimberti, M.-P. Gaigeot, M. Bonn, and E. H. G. Backus, "Molecular hydrophobicity at a macroscopically hydrophilic surface," Proc. Natl. Acad. Sci. U. S. A. **116**, 1520 (2019).
[27]S. Singla, E. Anim-Danso, A. E. Islam, Y. Ngo, S. S. Kim, R. R. Naik, and A. Dhinojwala, "Insight on structure of water and ice next to graphene using surface-sensitive spectroscopy," ACS Nano **11**, 4899 (2017).
[28]A. Myalitsin, S.-h. Urashima, S. Nihonyanagi, S. Yamaguchi, and T. Tahara, "Water structure at the buried silica/aqueous interface studied by heterodyne-detected vibrational sum-frequency generation," J. Phys. Chem. C **120**, 9357 (2016).
[29]M. Sulpizi, M. Salanne, M. Sprik, and M.-P. Gaigeot, "Vibrational sum frequency generation spectroscopy of the water liquid–vapor interface from density functional theory-based molecular dynamics simulations," J. Phys. Chem. Lett. **4**, 83 (2013).
[30]Y.-C. Wen, S. Zha, X. Liu, S. Yang, P. Guo, G. Shi, H. Fang, Y. R. Shen, and C. Tian, "Unveiling microscopic structures of charged water interfaces by surface-specific vibrational spectroscopy," Phys. Rev. Lett. **116**, 016101 (2016).
[31]S. Pezzotti, D. R. Galimberti, Y. R. Shen, and M.-P. Gaigeot, "Structural definition of the BIL and DL: A new universal methodology to rationalize non-linear $\chi^{(2)}(\omega)$ SFG signals at charged interfaces, including $\chi^{(3)}(\omega)$ contributions," Phys. Chem. Chem. Phys. **20**, 5190 (2018).
[32]S. Pezzotti, D. R. Galimberti, and M.-P. Gaigeot, "Deconvolution of BIL-SFG and DL-SFG spectroscopic signals reveals order/disorder of water at the elusive aqueous silica interface," Phys. Chem. Chem. Phys. **21**, 22188 (2019).
[33]S. K. Reddy, R. Thiraux, B. A. Wellen Rudd, L. Lin, T. Adel, T. Joutsuka, F. M. Geiger, H. C. Allen, A. Morita, and F. Paesani, "Bulk contributions modulate the sum-frequency generation spectra of water on model sea-spray aerosols," Chem **4**, 1629 (2018).
[34]S. Sun, F. Tang, S. Imoto, D. R. Moberg, T. Ohto, F. Paesani, M. Bonn, E. H. G. Backus, and Y. Nagata, "Orientational distribution of free O–H groups of interfacial water is exponential," Phys. Rev. Lett. **121**, 246101 (2018).
[35]T. Seki, S. Sun, K. Zhong, C.-C. Yu, K. Machel, L. B. Dreier, E. H. G. Backus, M. Bonn, and Y. Nagata, "Unveiling heterogeneity of interfacial water through the water bending mode," J. Phys. Chem. Lett. **10**, 6936 (2019).
[36]Y. Ni, S. M. Gruenbaum, and J. L. Skinner, "Slow hydrogen-bond switching dynamics at the water surface revealed by theoretical two-dimensional sum-frequency spectroscopy," Proc. Natl. Acad. Sci. U. S. A. **110**, 1992 (2013).
[37]L. Cheng, P. Fenter, K. L. Nagy, M. L. Schlegel, and N. C. Sturchio, "Molecular-scale density oscillations in water adjacent to a mica surface," Phys. Rev. Lett. **87**, 156103 (2001).

[38]S.-H. Park and G. Sposito, "Structure of water adsorbed on a mica surface," Phys. Rev. Lett. **89**, 085501 (2002).
[39]S. Kerisit, "Water structure at hematite–water interfaces," Geochim. Cosmochim. Acta **75**, 2043 (2011).
[40]J. G. Catalano, "Weak interfacial water ordering on isostructural hematite and corundum (001) surfaces," Geochim. Cosmochim. Acta **75**, 2062 (2011).
[41]A. P. Willard and D. Chandler, "Instantaneous liquid interfaces," J. Phys. Chem. B **114**, 1954 (2010).
[42]A. P. Willard and D. Chandler, "The molecular structure of the interface between water and a hydrophobic substrate is liquid-vapor like," J. Chem. Phys. **141**, 18C519 (2014).
[43]J. Kessler, H. Elgabarty, T. Spura, K. Karhan, P. Partovi-Azar, A. A. Hassanali, and T. D. Kühne, "Structure and dynamics of the instantaneous water/vapor interface revisited by path-integral and *ab initio* molecular dynamics simulations," J. Phys. Chem. B **119**, 10079 (2015).
[44]P. Tarazona and E. Chacón, "Monte Carlo intrinsic surfaces and density profiles for liquid surfaces," Phys. Rev. B **70**, 235407 (2004).
[45]E. Chacón and P. Tarazona, "Intrinsic profiles beyond the capillary wave theory: A Monte Carlo study," Phys. Rev. Lett. **91**, 166103 (2003).
[46]F. Bresme, E. Chacón, and P. Tarazona, "Molecular dynamics investigation of the intrinsic structure of water–fluid interfaces via the intrinsic sampling method," Phys. Chem. Chem. Phys. **10**, 4704 (2008).
[47]E. Chacón, E. M. Fernández, D. Duque, R. Delgado-Buscalioni, and P. Tarazona, "Comparative study of the surface layer density of liquid surfaces," Phys. Rev. B **80**, 195403 (2009).
[48]R. Šolc, M. H. Gerzabek, H. Lischka, and D. Tunega, "Wettability of kaolinite (001) surfaces—Molecular dynamic study," Geoderma **169**, 47 (2011).
[49]F. S. Emami, V. Puddu, R. J. Berry, V. Varshney, S. V. Patwardhan, C. C. Perry, and H. Heinz, "Force field and a surface model database for silica to simulate interfacial properties in atomic resolution," Chem. Mater. **26**, 2647 (2014).
[50]L. T. Zhuravlev, "The surface chemistry of amorphous silica: Zhuravlev model," Colloids Surf., A **173**, 1 (2000).
[51]D. L. Bish, "Rietveld refinement of the kaolinite structure at 1.5 K," Clays Clay Miner. **41**, 738 (1993).
[52]N. R. Haria, G. S. Grest, and C. D. Lorenz, "Viscosity of nanoconfined water between hydroxyl basal surfaces of kaolinite: Classical simulation results," J. Phys. Chem. C **117**, 6096 (2013).
[53]S. A. Zielke, A. K. Bertram, and G. N. Patey, "Simulations of ice nucleation by kaolinite (001) with rigid and flexible surfaces," J. Phys. Chem. B **120**, 1726 (2016).
[54]H. J. C. Berendsen, J. R. Grigera, and T. P. Straatsma, "The missing term in effective pair potentials," J. Phys. Chem. **91**, 6269 (1987).
[55]M. G. Martin and J. I. Siepmann, "Transferable potentials for phase equilibria. 1. United-atom description of *n*-alkanes," J. Phys. Chem. B **102**, 2569 (1998).
[56]R. T. Cygan, J.-J. Liang, and A. G. Kalinichev, "Molecular models of hydroxide, oxyhydroxide, and clay phases and the development of a general force field," J. Phys. Chem. B **108**, 1255 (2004).
[57]T. Darden, D. York, and L. Pedersen, "Particle mesh Ewald: An *N* log (*N*) method for Ewald sums in large systems," J. Chem. Phys. **98**, 10089 (1993).
[58]U. Essmann, L. Perera, M. L. Berkowitz, T. Darden, H. Lee, and L. G. Pedersen, "A smooth particle mesh Ewald method," J. Chem. Phys. **103**, 8577 (1995).
[59]M. J. Abraham, T. Murtola, R. Schulz, S. Páll, J. C. Smith, B. Hess, and E. Lindahl, "GROMACS: High performance molecular simulations through multi-level parallelism from laptops to supercomputers," SoftwareX **1-2**, 19 (2015).
[60]W. G. Hoover, "Canonical dynamics: Equilibrium phase-space distributions," Phys. Rev. A **31**, 1695 (1985).
[61]S. Nosé, "A molecular dynamics method for simulations in the canonical ensemble," Mol. Phys. **52**, 255 (1984).
[62]S. Nosé and M. L. Klein, "Constant pressure molecular dynamics for molecular systems," Mol. Phys. **50**, 1055 (1983).
[63]M. Parrinello and A. Rahman, "Polymorphic transitions in single crystals: A new molecular dynamics method," J. Appl. Phys. **52**, 7182 (1981).
[64]S. Han, P. Kumar, and H. E. Stanley, "Absence of a diffusion anomaly of water in the direction perpendicular to hydrophobic nanoconfining walls," Phys. Rev. E **77**, 030201 (2008).
[65]L. F. Mercier Franco, M. Castier, and I. G. Economou, "Diffusion in homogeneous and in inhomogeneous media: A new unified approach," J. Chem. Theory Comput. **12**, 5247 (2016).
[66]D. Laage and J. T. Hynes, "A molecular jump mechanism of water reorientation," Science **311**, 832 (2006).
[67]S. A. Safran, *Statistical Thermodynamics of Surfaces, Interfaces, and Membranes* (Addison-Wesley, Reading, MA, 1994).
[68]P.-L. Chau and A. J. Hardwick, "A new order parameter for tetrahedral configurations," Mol. Phys. **93**, 511 (1998).
[69]Y. Zhang, H. B. de Aguiar, J. T. Hynes, and D. Laage, "Water structure, dynamics, and sum-frequency generation spectra at electrified graphene interfaces," J. Phys. Chem. Lett. **11**, 624 (2020).
[70]M. Bonn, Y. Nagata, and E. H. G. Backus, "Molecular structure and dynamics of water at the water–air interface studied with surface-specific vibrational spectroscopy," Angew. Chem., Int. Ed. **54**, 5560 (2015).
[71]D. E. Moilanen, N. E. Levinger, D. B. Spry, and M. D. Fayer, "Confinement or the nature of the interface? Dynamics of nanoscopic water," J. Am. Chem. Soc. **129**, 14311 (2007).
[72]R. Delgado-Buscalioni, E. Chacón, and P. Tarazona, "Capillary waves' dynamics at the nanoscale," J. Phys.: Condens. Matter **20**, 494229 (2008).
[73]S. Romero-Vargas Castrillón, N. Giovambattista, I. A. Aksay, and P. G. Debenedetti, "Evolution from surface-influenced to bulk-like dynamics in nanoscopically confined water," J. Phys. Chem. B **113**, 7973 (2009).
[74]M. Chen, X. Lu, X. Liu, Q. Hou, Y. Zhu, and H. Zhou, "Slow dynamics of water confined in Newton black films," Phys. Chem. Chem. Phys. **17**, 19183 (2015).
[75]A. C. Fogarty, E. Duboué-Dijon, D. Laage, and W. H. Thompson, "Origins of the non-exponential reorientation dynamics of nanoconfined water," J. Chem. Phys. **141**, 18C523 (2014).
[76]W. H. Thompson, "Perspective: Dynamics of confined liquids," J. Chem. Phys. **149**, 170901 (2018).
[77]F. G. J. Longford, J. W. Essex, C.-K. Skylaris, and J. G. Frey, "Surface reconstruction amendment to the intrinsic sampling method," J. Chem. Phys. **149**, 234705 (2018).
[78]R. Godawat, S. N. Jamadagni, and S. Garde, "Characterizing hydrophobicity of interfaces by using cavity formation, solute binding, and water correlations," Proc. Natl. Acad. Sci. U. S. A. **106**, 15119 (2009).
[79]S. N. Jamadagni, R. Godawat, and S. Garde, "Hydrophobicity of proteins and interfaces: Insights from density fluctuations," Annu. Rev. Chem. Biomol. Eng. **2**, 147 (2011).
[80]A. P. Gaiduk, T. A. Pham, M. Govoni, F. Paesani, and G. Galli, "Electron affinity of liquid water," Nat. Commun. **9**, 247 (2018).
[81]C.-S. Hsieh, R. K. Campen, M. Okuno, E. H. G. Backus, Y. Nagata, and M. Bonn, "Mechanism of vibrational energy dissipation of free OH groups at the air–water interface," Proc. Natl. Acad. Sci. U. S. A. **110**, 18780 (2013).
[82]E. Lindahl and O. Edholm, "Mesoscopic undulations and thickness fluctuations in lipid bilayers from molecular dynamics simulations," Biophys. J. **79**, 426 (2000).
[83]M. Chen, X. Lu, X. Liu, Q. Hou, Y. Zhu, and H. Zhou, "Specific counterion effects on the atomistic structure and capillary-waves fluctuation of the water/vapor interface covered by sodium dodecyl sulfate," J. Phys. Chem. C **118**, 19205 (2014).